Journal of the Brazilian Society of Mechanical Sciences and Engineering (2018) 40:72
https://doi.org/10.1007/s40430-018-0962-6

TECHNICAL PAPER

Direct ethanol fuel cell as aircraft APU: a study for onboard waste heat recovery

Marcelo de Almeida Ramsdorf[1] · José Alexandre Matelli[2]

Received: 30 June 2017 / Accepted: 3 January 2018 / Published online: 23 January 2018

Abstract

An advanced concept of jet aircraft (known as "more electric aircraft") available nowadays requires electrically driven systems. In this scenario, application of low-temperature fuel cells in aircraft is an interesting alternative to generate power for the electrically driven systems with high efficiency and low environment impact. However, hydrogen fuel cells pose difficulties for aircraft designers due to safety and weight requirements related to onboard use of hydrogen. Direct ethanol polymer fuel cells (DEPFC) may overcome such difficulties, but recent publications show that DEPFC still presents low efficiency and, therefore, generates high amounts of waste heat. In this work, the use of a DEPFC as auxiliary power unit (APU) in a regional jet is proposed and opportunities for onboard waste heat recovery are evaluated. Obtained results suggest that heat recovery from DEPFC is technically feasible for cabin heating, fuel heating, and water onboard production.

Keywords Fuel cell · Ethanol · Aircraft · Heat recovery

Abbreviations

APU	Auxiliary power unity
DEPFC	Direct ethanol polymeric fuel cell
GDL	Gas-diffusion layer
PEMFC	Polymer electrolyte membrane fuel cell
SOFC	Solid oxide fuel cell

Nomenclature

C	Concentration (kmol l^{-1})
c_p	Specific heat (kJ kg^{-1} K^{-1})
D_{EtOH}	Ethanol–water diffusion coefficient (cm^2 s^{-1})
D_{O_2}	Oxygen-water vapor diffusion coefficient (cm^2 s^{-1})
E	Cell potential (V)
e	Specific molar exergy (kJ $kmol^{-1}$)
$\dot{E}x$	Exergy rate (kW)
F	Faraday's constant, (96,485 kC $kmol^{-1}$)
G	Gibb's free energy (kJ)
H	Enthalpy (kJ)
h	Specific molar enthalpy (kJ $kmol^{-1}$)
I	Irreversibility (kW)
i	Current density (mA cm^{-1})
K_{EtOH}	Lumped parameter for ethanol oxidation (C $mol^{-0.5}cm^{-0.5}s^{-1}$)
$k_{c,fc}$	Cell effective conductivity (S cm^{-1})
k_d	Mass transport coefficient of ethanol in the diffusion layer (cm s^{-1})
k_f	Mass transport coefficient from feed ethanol stream to the diffusion layer (cm s^{-1})
L_c	Catalyst layer thickness (cm)
L_d	Gas-diffusion layer thickness (cm)
L_m	Membrane thickness (cm)
M	Molar mass of water (kg $kmol^{-1}$)
$\dot{m}$	Mass flow rate (kg s^{-1})
N	Number of samples
$\dot{n}$	Molar flow rate (kmol s^{-1})
P	Pressure (atm, Pa)
$\dot{Q}$	Heat transfer rate (kW)
R	Universal gas constant (8.314 kJ $kmol^{-1}$ K^{-1})
R_b	Contact specific resistance (Ω cm^2)
s	Specific molar entropy (kJ $kmol^{-1}$ K^{-1})

Technical Editor: Jose A. dos Reis Parise.

✉ José Alexandre Matelli
matelli@feg.unesp.br

Marcelo de Almeida Ramsdorf
marcelo.ramsdorf@anac.gov.br

[1] National Civil Aviation Agency (ANAC), São José Dos Campos, SP, Brazil

[2] Department of Energy, School of Engineering, São Paulo State University (UNESP), Guaratinguetá, SP, Brazil

T	Temperature (K)
V	Cell voltage (V)
v_d	Superficial velocity of water in the diffusion layer (cm s^{-1})
W_{el}^0	Maximum work generated by the fuel cell (kJ)
$\dot{W}_{el}$	Cell power output (kW)
X	Molar fraction
z	Number of released electrons in fuel cell ideal reaction (kmol)

Greek symbols

α	Transfer coefficient
β_{H_2O}	Electro-osmotic drag coefficient of water
γ	Excess air coefficient
ε	Average deviation
ε_d	Gas-diffusion layer void fraction
λ	Cell overpotential (V)
ρ	Specific mass (kg m^{-3})
σ_m	Membrane conductivity (Ω^{-1} cm^{-1})
ψ	Rational efficiency

Subscripts

0	Reference conditions
a	Anode
c	Cathode, concentration
fc	Fuel cell
N	Nernst
oh	Ohmic
ph	Physical
ch	Chemical
out	Output
in	Input
i	Material stream i
j	Chemical species j

Superscripts

0	Reference conditions, maximum

1 Introduction

Development of non-pollutant, efficient, and safe energy conversion technologies for vehicular use (automobiles, buses, trucks, trains, ships, and aircraft) is a critical issue. Conversion of fuel chemical energy into power or mechanical work with no production of pollutant gases, especially NOx, is virtually impossible when using thermal engines, such as reciprocating internal combustion engines or gas turbines. In particular, aviation industry is a major contributor to air pollution around airports and in the troposphere [1–4]. In this scenario, fuel cells are an interesting alternative for power generation in aircraft due to its high efficiency and low environment impact. Indeed, it can be found in the technical literature works approaching the use of fuel cell either for aircraft propulsion [5–8] or for auxiliary onboard power generation [9–13]. All these works considered fuel cells fed by hydrogen, either pure or produced by reforming. In any case, onboard use of hydrogen still poses difficulties for aircraft application due to safety and weight requirements.

Ethanol is a renewable fuel largely available in countries like Brazil and is an interesting alternative for aviation. Indeed, EMB 202 Ipanema, from Brazilian manufacturer Embraer, is an ethanol-fueled airplane commercially available for agricultural application. In this context, direct ethanol polymer fuel cell (DEPFC) can overcome the difficulties related to hydrogen. Ethanol fuel cells still present low efficiency and high generation of waste heat, so that state-of-the-art research concentrates on membrane construction and non-platinum catalyst [14, 15].

Depending on how rationally DEPFC waste heat is managed, it can be a promising technology for power generation on board jet aircraft, especially those known as "more electric aircraft". A comparison between a conventional aircraft and a more electric one is shown in Fig. 1. Conventional aircraft, such as the Boeing 737, has most of its systems based on bleed air, i.e., high pressure air extracted from the auxiliary power unit (APU) or the main engines. On the other hand, in a more electric aircraft, such as the Boeing 787, bleed air is used only for engine anti-icing. All other embedded systems, except the hydraulic one, relay on power.

In this work, the use of a DEPFC as APU in a regional jet reconfigured as more electric is proposed. First, power and heat demands of the jet on all stages of a flight are estimated based on literature. The fuel cell is then modelled and sized to meet the power demand. Waste heat is calculated and an exergetic analysis is performed to evaluate opportunities for onboard heat recovery. The application of DEPFC as APU and its exergetic analysis are original contributions of this work.

2 Methodology

2.1 Energy demands of a regional jet

Santarelli and Cabrera [12] found the Dornier 328 regional jet well suited for reconfiguration more electric and proposed an onboard solid oxide fuel cell as APU. The authors also provided a very detailed analysis of the jet energy demands during all flight phases, as shown in Fig. 2. In the present work, it is considered the same jet and the same flight, so that a DEPFC is sized to meet the aircraft energy demands, as shown in Fig. 2. It is important to note that, unlike Boing 787, cabin pressurization of the Dornier 328

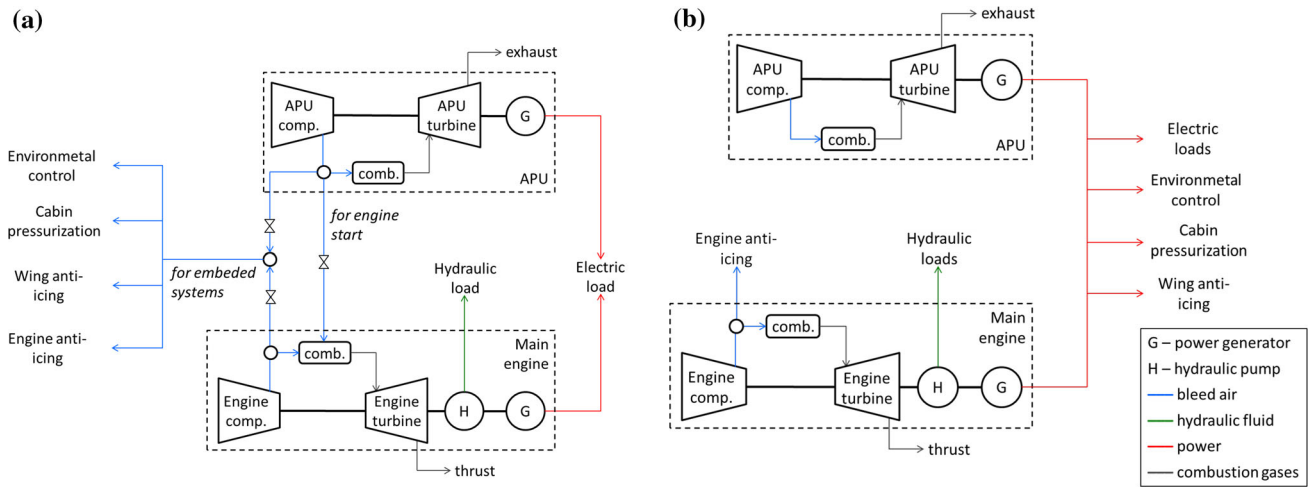

Fig. 1 Conventional aircraft (**a**) and more electric aircraft (**b**)

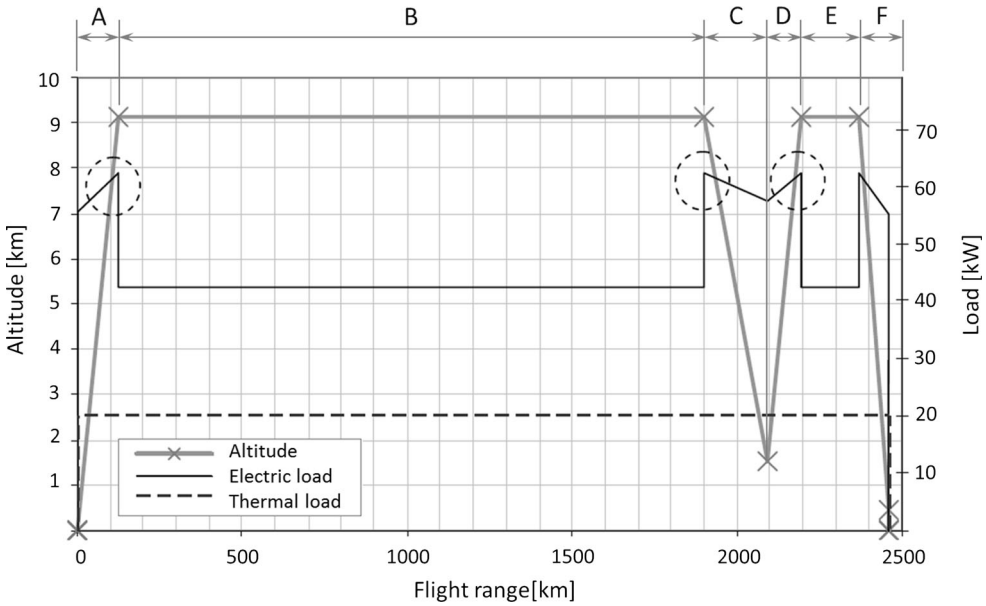

Fig. 2 Power and thermal demands of a regional jet (Reproduced with permission from [12])

is provided by bleed air from the main engines and it is not accounted as a power demand of this aircraft.

Regarding thermal load, the jet requires 20 kW of power for cabin heating during all flight. For other systems, peak demand of power, about 62.5 kW, occurs during climb after takeoff and descent for landing. Figure 2 shows the flight divided in six stages. Stages D, E, and F represent a missed approach followed by climb, cruise, and descent to land in an alternate airfield. Note that the power peak occurs in stages A, C, D, and F, because the electric wing anti-icing system is turned on to cross high-humidity, low-temperature regions that favors ice formation. Thus, during climb after takeoff and descent for landing, cabin heating, air conditioning, wing anti-icing, and other electric loads (lights, avionics, etc.) demand 82.5 kW of power. The DEPFC should then be sized to meet this demand, so that a model to predict the fuel cell performance is presented in the next section.

2.2 DEPFC model

The electrochemical process of a DEPFC is composed of ethanol oxidation in anode (Eq. 1) and oxygen reduction in cathode (Eq. 2), resulting in the cell global reaction (Eq. 3). A typical scheme of a DEPFC is shown in Fig. 3. Ethanol and water are admitted in the anode. Ions H^+ pass through the membrane to the cathode, electrons are released through the bipolar plate, and carbon dioxide is exhausted. On the cathode side, oxygen is admitted and reacts with ions H^+ from membrane and the electrons from bipolar plate. The power generated by the cell corresponds to the flow of electrons between the anode and cathode

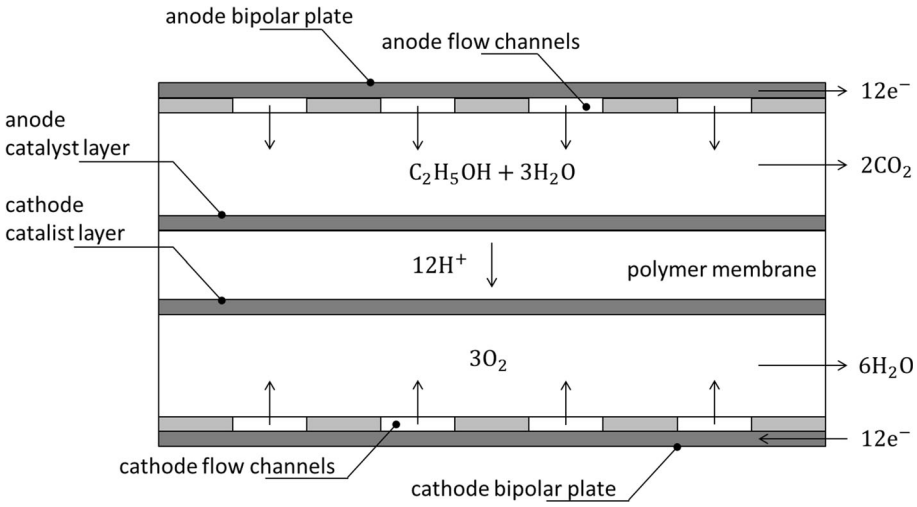

Fig. 3 DEPFC scheme

bipolar plates. Both anode and cathode reactions require catalysis, so that catalyst layers are provided:

$$C_2H_5OH + 3H_2O \rightarrow 12H^+ + 12e^- + 2CO_2 \quad (1)$$

$$12H^+ + 3O_2 + 12e^- \rightarrow 6H_2O \quad (2)$$

$$C_2H_5OH + 3O_2 + 3H_2O \rightarrow 2CO_2 + 6H_2O. \quad (3)$$

In real-world DEPFC operation, highly humid air should be admitted in cathode instead of pure oxygen. The need for humidity is to avoid polymer membrane drying, which is the reason why cell temperature should not exceed 100 °C. Polymer membrane also must present an adequate barrier to mixing of fuel and reactant gases [16], a major factor that contributes to DEPFC low efficiency and quantified as crossover overpotential. Typically, a DEPFC fuel cell uses Nafion modified with KOH as membrane, carbon paper GDL, and palladium-based catalyst on both anode and cathode [21]. Thickness of membrane, GDL, and catalyst layers are considered in the model presented here, as detailed ahead in this section.

At standard conditions, the maximum work generated by a fuel cell equals the Gibbs free energy of the cell global reaction, which is also related to the cell maximum potential E^0 (Eq. 4):

$$W_{el}^0 = -\Delta G^0 = zFE^0. \quad (4)$$

The Gibbs free energy at cell conditions can be calculated through the Gibbs–Helmholtz equation (Eq. 5), so that the Nernst potential at cell conditions is calculated through Eq. 6:

$$\Delta G(T_{fc}, P_{fc}) = T_{fc}\left[\frac{\Delta G^0}{T_0} + \Delta H^0\left(\frac{1}{T_{fc}} - \frac{1}{T_0}\right)\right] \quad (5)$$

$$E_N(T_{fc}, P_{fc}) = -\Delta G(T_{fc}, P_{fc})/(zF). \quad (6)$$

Overpotential decreases the Nernst potential of a cell. In this work, the overpotentials of a DEPFC are modelled based on the works of Pramanik and Basu [16], Andreadis et al. [17], Abdullah et al. [18], Goel and Basu [19], and Sousa et al. [20]. According to these authors, fuel cell potential may be modelled considering activation overpotential in the anode ($\lambda_{a,a}$), concentration overpotential in both anode ($\lambda_{c,a}$) and cathode ($\lambda_{c,c}$), and the ohmic overpotential (λ_{oh}) due to the membrane conductivity and plates resistivity. Activation overpotential in the cathode is not considered, because it is less significant compared to that at anode, since it is well reported in the literature that the oxygen reduction kinetics on Pt electrocatalyst is excellent compared to ethanol electro-oxidation on Pt-based electrocatalyst [16]. Crossover overpotential is not explicitly considered in the model. Instead, as proposed by Andreadis et al. [17], it is accounted in the cathode concentration overpotential as an inefficiency-related electron release by the cathode reaction. Thus, the actual cell potential is calculated by Eq. 7 and each overpotential is described in details ahead:

$$V_{fc} = E_N(T_{fc}, P_{fc}) - \lambda_{a,a} - \lambda_{c,a} - \lambda_{c,c} - \lambda_{oh}. \quad (7)$$

2.3 Anode activation overpotential

Actual DEPFC exhausts also unreacted ethanol, water, acetic acid, and acetaldehyde in the anode. Consequently, not all of the 12 electrons are released straight to the external circuit due to the strong C–C bond. It can be assumed that a mean of 4 mols of electrons are transferred during the ethanol oxidation [17] to form reaction products. The activation overpotential in the anode can be estimated by the following equation [19]:

$$\lambda_{a,a} = \frac{R\ T_{fc}}{\alpha_a F z_a} \ln\left[\frac{i\ (C_{EtOH})^{-0.25}(C_{H_2O})^{-0.25}}{K_{EtOH}}\right]. \quad (8)$$

2.4 Anode concentration overpotential

Mass transport resistance through the anode is affected by the ethanol concentration, resulting in the anode concentration overpotential expressed by Eq. 9 [16]. In this equation, k_f is the mass transfer coefficient from the feed ethanol stream to the diffusion layer (Eq. 10); k_d is the mass transfer coefficient of ethanol in the diffusion layer (Eq. 11); and v_d is the superficial velocity of water in the diffusion layer (Eq. 12):

$$\lambda_{c,a} = \frac{R\ T_{fc}}{\alpha_a F z_a} \ln \left\{ \frac{i}{i_0} \left[\exp\left(\frac{v_d}{k_d}\right) + \frac{i}{z_a F v_d C_{EtOH} \left[\exp\left(\frac{v_d}{k_d}\right)\left(\frac{v_d}{k_f}+1\right) - 1 \right]} \right]^{-1} \right\} \quad (9)$$

$$k_f = 1.87 \times 10^{-4} \left(\frac{i}{0.003}\right)^{0.32} \quad (10)$$

$$k_d = \frac{D_{EtOH}(\varepsilon_d)^{3/2}}{L_d} \quad (11)$$

$$v_d = \frac{M_{H_2O} i}{\rho_{H_2O} F} \left(\frac{1}{z_a} + \beta_{H_2O}\right). \quad (12)$$

2.5 Cathode concentration overpotential

According to Andreadis et al. [17], oxygen reduction reaction in the cathode transfers 1 mol of electrons instead of 4 mol predicted in stoichiometric reaction (Eq. 2), which leads to an efficiency reduction. Pramanik and Basu [16] explain that the oxygen partial pressure reduction also induces the concentration overpotential and provides Eq. (13) to predict the cathode concentration overpotential:

$$\lambda_{c,c} = \frac{R\ T_{fc}}{\alpha_c F z_c} \ln\left(\frac{i}{i_0[1 - iJ]}\right), \quad (13)$$

where J is a constant defined by the following equation:

$$J = \frac{L_d C_{O_2}}{z_c F D_{O_2} (\varepsilon_d)^{3/2}}. \quad (14)$$

2.6 Ohmic overpotential

Ohmic overpotential is related to membrane conductivity σ_m ($\Omega^{-1}cm^{-1}$) and contact resistance. This resistance refers to the losses between the contacts of the fuel cell components [17]. Goel and Basu [19] estimated the membrane conductivity according to Eq. 15 and Abdullah et al. [18] presented the contact overpotential through Eq. 16. The Nafion reference conductivity of 0.073 S cm in Eq. 15 was provided by measurements of Goel and Basu [19] at 25 °C:

$$\sigma_m = 0.073 \exp\left[1268\left(\frac{1}{298} - \frac{1}{T_{fc}}\right)\right] \quad (15)$$

$$\lambda_{oh} = i\left(\frac{L_m}{\sigma_m} + \frac{L_m + 2L_c + 2L_d}{k_{c,ef}}\right). \quad (16)$$

2.7 Limiting current density and model parameters

As a result of mass transport limitation of ethanol and oxygen, current density of a DEPFC is limited in the anode and in the cathode, respectively. It means that the cell cannot operate above these limits, because the ion transportation through the membrane ceases [17]. Theoretical estimative for limiting currents in anode (Eq. 17) and cathode (Eq. 18) is provided by Andreadis et al. [17]:

$$i^*_{EtOH} = \frac{z_a F D_{EtOH} (\varepsilon_d)^{3/2} C_{EtOH}}{L_d} \quad (17)$$

$$i^*_{O_2} = \frac{z_c F D_{O_2} (\varepsilon_d)^{3/2} C_{O_2}}{L_d}. \quad (18)$$

Table 1 provides a summary of the parameters taken from the literature that are used in the DEPFC proposed model.

2.8 Onboard DEPFC stack

Modules are composed of individual fuel cells connected through the bipolar plates to compose a stack that provides direct current in the same way that an APU does. Individual fuel cells are connected in series to produce the desired voltage, forming the modules. Modules are to be connected in parallel to obtain the total power for the systems. This arrangement depends on the power demand and tension of the aircraft circuits. Power density of the cells is a crucial parameter for aeronautic applications due to its relation to the stack weight. At higher power densities, the stack could be smaller (smaller area) and lighter; however, the cell could not work depending on the current density due to the mass transport limitation above the limiting current, as described in Sect. 2.3. Furthermore, DEPFC generates high amount of waste heat at higher power densities, which must be properly managed to avoid membrane drying [21]. On the other hand, at low power densities, the stack would become larger and heavier. According to Andreadis et al. [17], a DEPFC with PtRu/C as anode electrode, Pt/C as cathode electrode, and Nafion 115 membrane as electrolyte reach the maximum power density when its current density is about 100 mA/cm^2.

Table 1 DEPFC model parameters

Parameter	Description	Value	References
C_{EtOH}	Ethanol concentration	0.001 mol ml^{-1}	[16]
C_{O_2}	Oxygen concentration at air–GDL interface	0.3289×10^{-6} mol ml^{-1}	[19]
D_{EtOH}	Diffusion coefficient of ethanol in water	1.83×10^{-5} cm^2s^{-1}	[22]
D_{O_2}	Diffusion coefficient of oxygen in water vapor	0.357 cm^2s^{-1}	[22]
i_0	Exchange current density at anode and cathode	0.136 mA cm^{-2} @ 75 °C	[22]
		0.680 mA cm^{-2} @ 90 °C	
K_{EtOH}	Lumped parameter for ethanol oxidation	1 C $mol^{-0.5}cm^{-0.5}s^{-1}$	[22]
$k_{c,ef}$	Cell effective conductivity	0.07 S cm^{-1}	[22]
L_c	Catalyst layer thickness	0.001 cm	[22]
L_d	GDL thickness	0.03 cm	[22]
L_m	Membrane thickness	0.00145 cm	[22]
z_a	Number of electrons released in anode reaction	4 mol	[17]
z_c	Number of electrons released in cathode reaction	1 mol	[17]
α_a	Anode transfer coefficient	0.089	[18]
α_c	Cathode transfer coefficient	1	[18]
ε_d	GDL void fraction*	0.834	[16]
β_{H_2o}	Electro-osmotic drag coefficient of water	3.16	[16]

Stack operation conditions are as follows. Stack pressure is 1 atm, so that maximum operation temperature is limited to 90 °C to avoid membrane water evaporation. Aqueous solution of ethanol with ethanol molar fraction of 0.25 feeds the stack. Current density is kept constant and equal to 100 mA/cm^{-2} [17]. Cabin air as the source of oxygen in fuel cell stacks when in high altitudes instead of external air; otherwise, an extra air compressor would require more power from the stack, increasing its weight and size. It is safe to assume that air is admitted at 25 °C, and it is volume fraction is 21% of oxygen and 79% of nitrogen. It is considered that cathode inlet air stream provides 50% more oxygen than the stoichiometric oxygen required in cathode reaction ($\gamma = 1.5$). Ethanol and oxygen consumption are given in Eqs. 19 and 20, respectively. Water and CO_2 generation are given in Eqs. 21 and 22. Equations 19–22 are molar-based and are adapted to take into account Faraday's Law. Cell efficiency based on the cell global reaction enthalpy ($\Delta H^0 = 1367$ MJ/kmol) is given in Eq. 23:

$$\dot{n}_{in}^{EtOH} = \frac{\dot{W}_{el}}{12V_{fc}F} \tag{19}$$

$$\dot{n}_{in}^{O_2} = \gamma\frac{\dot{W}_{el}}{4V_{fc}F} \tag{20}$$

$$\dot{n}_{out}^{CO_2} = \frac{\dot{W}_{el}}{4V_{fc}F} \tag{21}$$

$$\dot{n}_{out}^{H_2O} = \frac{\dot{W}_{el}}{2V_{fc}F} \tag{22}$$

$$\eta_{fc} = \frac{\dot{W}_{el}}{\dot{n}_{in}^{EtOH}\Delta H^0} = \frac{12V_{fc}F}{\Delta H^0}. \tag{23}$$

The APU composed of a DEPFC stack and its subsystems is depicted in Fig. 4. It is assumed that only CO_2 is formed in the ethanol electro-oxidation and that ethanol remains in liquid state. Ethanol (point 1) and air (point 2) are admitted at ambient temperature. Electrochemical reactions in the anode stack results in CO_2 and unreacted ethanol (point 3), as long as cathode reactions results in H_2O and unreacted O_2 and N_2 (point 4). Aqueous ethanol (point 7) is separated from the CO_2 (point 5) and reutilized

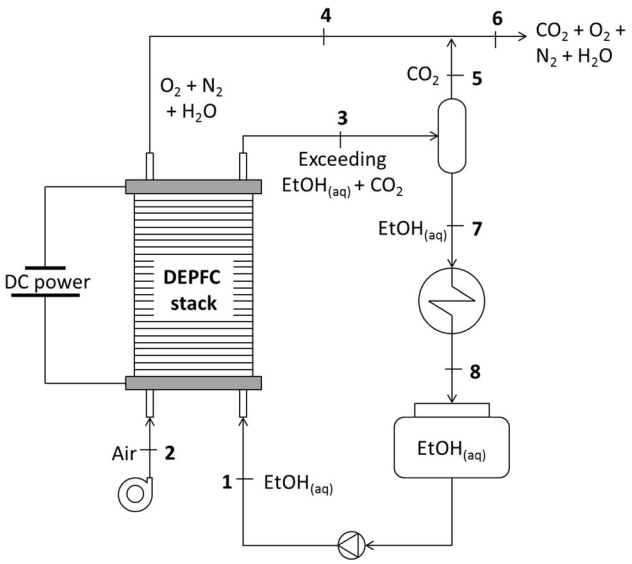

Fig. 4 APU composed of a DEPFC stack and subsystems

after cooling (point 8). Stack exhaust (point 6) is formed from separated CO_2 (point 5) and cathode exhaust (point 4).

2.9 Exergy analysis

Exergy analysis is carried out to evaluate opportunities for heat recovery from the DEPFC stack. Heat generated due to the cell overpotentials is calculated according to Eq. 24. The heat of a material stream i composed of different j species is determined according to Eq. 25:

$$\dot{Q}_{\lambda} = \dot{W}_{el}\left[\frac{E_N(T_{fc}, P_{fc})}{V_{fc}} - 1\right] \tag{24}$$

$$\dot{Q}_i = \sum_j \dot{n}_j(\bar{h}_j - \bar{h}_{j,0}). \tag{25}$$

In this work, all gases are considered ideal gases. When considering a material stream i composed of a mixture of j substances, exergy can be split into physical and chemical parts (Eq. 26). Physical exergy (Eq. 27) of a material stream i composed of j substances requires calculation of stream's enthalpy and entropy (Eqs. 28 and 29, respectively):

$$\bar{e}_i = \bar{e}_{ph,i} + \bar{e}_{ch,i} \tag{26}$$

$$\bar{e}_{ph,i} = \left(\bar{h}_i - \bar{h}_{i,0}\right) - T_0\left(\bar{s}_i - \bar{s}_{i,0}\right) \tag{27}$$

$$\bar{h}_i = \sum_j X_j \bar{h}_j \tag{28}$$

$$\bar{s}_i = \sum_j X_j \bar{s}_j. \tag{29}$$

Chemical exergy of a material stream i is split into standard chemical exergy (Eq. 30) of the j substances (Table 2) and the exergy related to the concentration of each j substance in a mixture of ideal gases (Eq. 31). Thus, total exergy rate of material stream i is determined according to Eq. 32:

$$\bar{e}^{S}_{ch,i} = \sum_j X_j \bar{e}^{0}_{ch,j} \tag{30}$$

$$\bar{e}^{C}_{ch,i} = \sum_j \bar{R} T_0 \ln(X_j) \tag{31}$$

Table 2 Specific exergy of pure substances [22]

j	Substance	$\bar{e}^{0}_{ch,j}$ [kJ/mol]
1	N_2	0.640
2	O_2	3.92
3	CO_2	20.2
4	$H_2O_{(l)}$	0.914
5	$C_2H_5OH_{(l)}$	1357

$$\dot{E}x_i = \dot{n}_i\left(\bar{e}_{ph,i} + \bar{e}_{ch,i}\right) = \dot{n}_i\left[\bar{e}_{ph,i} + \left(\bar{e}^{S}_{ch,i} + \bar{e}^{C}_{ch,i}\right)\right]. \tag{32}$$

Exergy related to work (or power) and heat is given in Eqs. 33 and 34, respectively:

$$\dot{E}x_w = \dot{W}_{el} \tag{33}$$

$$\dot{E}x_h = \left(1 - \frac{T_0}{T}\right)\dot{Q}. \tag{34}$$

Considering steady state, irreversibility related to the entropy generation is the difference between all the exergy that enters in a system/control volume and all the exergy that leaves it (Eq. 35). Rational efficiency (Eq. 36) measures how close a system is to its maximum efficiency: the higher its rational efficiency, the lower its entropy generation:

$$I = \sum \dot{E}x_{in} - \sum \dot{E}x_{out} \tag{35}$$

$$\psi = \frac{\sum \dot{E}x_{out}}{\sum \dot{E}x_{in}} = 1 - \frac{I}{\sum \dot{E}x_{in}}. \tag{36}$$

3 Results and discussion

3.1 Fuel cell model

Fuel cell model resulted in a system of equations solved with the Engineering Equation Solver (EES), a commercial software for solving systems of equations based on Newton–Raphson algorithm featuring a comprehensive thermodynamic database. For the considered DEPFC, Fig. 5a shows two polarization curves for different temperatures and Fig. 5b shows the power density.

For a given current density, it can be observed that both cell voltage and power density increase with temperature. This is expected, since the activation overpotential decreases with temperature. Theoretical limiting current resulted in 190 mA/cm^2. Obtained results are in good agreement with those presented in Sousa et al. [20], as shown in Fig. 6. When considering the whole current density range (1–120 mA/cm^2), average deviation from the experimental data found in the literature [20] (Eq. 37) are $\varepsilon = 6.46\%$ and $\varepsilon = 10.2\%$ for 75 °C and 90 °C, respectively. Disregarding the 1 mA/cm^2 point in both cases, average deviation is $\varepsilon = 5.43\%$ and $\varepsilon = 6.73\%$ for 75 °C and 90 °C, respectively.

$$\varepsilon = \frac{1}{N}\sum_{k=1}^{N}\frac{\left|V_{mod,k} - V_{exp,k}\right|}{V_{exp,k}}. \tag{37}$$

Figure 7a and b shows the linear regression between model results and experimental data from [20] in the range of 1–120 mA/cm^2 for 75 and 90 °C, resulting in

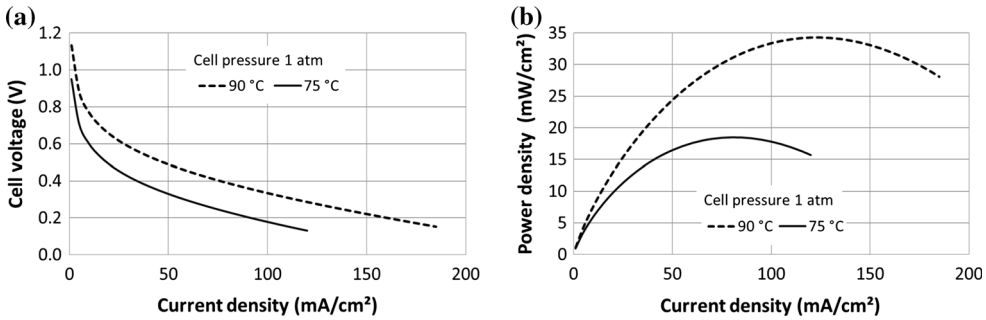

Fig. 5 **a** Polarization curve. **b** Power density

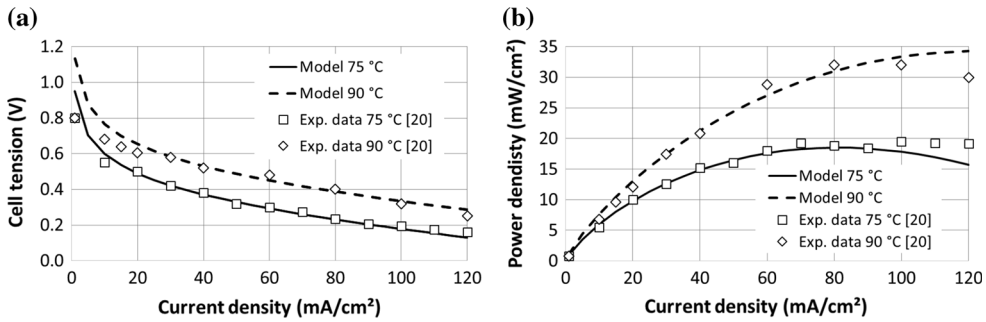

Fig. 6 Model versus experimental results from [20]: **a** polarization curve; **b** power density

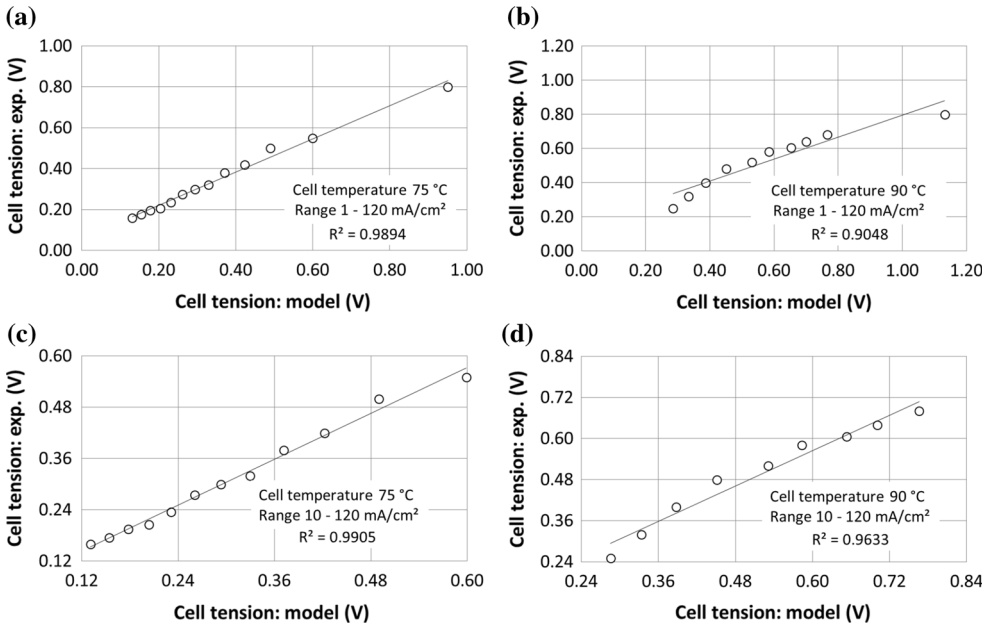

Fig. 7 Linear regression between model results and experimental data from [20]: **a** 75 °C, 1–120 mA/cm^2; **b** 90 °C, 1–120 mA/cm^2; **c** 75 °C, 10–120 mA/cm^2; **d** 90 °C, 10–120 mA/cm^2

$R^2 = 0.9736$ and $R^2 = 0.9736$, respectively. Figure 7c and d shows the same linear regression, but now disregarding the 1 mA/cm^2 point, resulting in $R^2 = 0.9736$ and $R^2 = 0.9736$ for 75 and 90 °C, respectively. Such results clearly indicate that the model presented here is appropriate to the DEPFC analysis within the current density range from 10 to 120 mA/cm^2.

3.2 Stack waste heat analysis

As the Nafion membrane needs liquid water, the maximum temperature of polymeric fuel cells is kept at 90 °C to avoid water evaporation at 1 atm [21]. For a current density of 100 mA/cm^2, cell tension and total overpotential result in 0.333 and 0.804 V, respectively, so that 144 individual cells must be serially connected to meet 48 V that the aircraft electric systems require. It is assumed a fuel utilization factor of 95%, a value 5.6% higher than the one

considered by Suresh and Jayanti [23], which achieved good results compared to the experimental data. Power density of each of these modules is 4.8 W/cm^2; for cells with 30 cm^2 of active area, the power output of each module is 144 W. Thus, 591 modules are required to meet 85 kW, which corresponds to the maximum power demand of the flight presented in Fig. 2. The total active area of this stack is about 255.5 m^2. Heat rejected by the stack due to cell overpotential is 205.5 kW. Table 3 summarizes the results previously presented, and Table 4 shows the mass and molar flow, thermodynamic state, and composition of each stream identified in Fig. 4. Supposing that the total volume of the stack is 130 L (about the same of a 40 × 40 × 80 cm^3 Honeywell 36–150 APU), it would lead to a vertical array of 7 per 7 modules piled horizontally in 12 columns, which would requires a cell thickness of 0.5 mm. Since this cell thickness is unrealistic, an actual stack would not fit in the APU nacelle. Abdullah et al. [18] present some estimation for anode catalyst, diffusion, and membrane layer thickness. It is required at least 1.7 mm of thickness for each cell, not considering the bipolar plates and the equivalent cathode layers. Thus, it is safe to state that a DEFC stack is currently less compact than a gas turbine-based APU of similar capacity. Moreover, Berg et al. [24] claim that "the present state-of-the-art for the DEFC technology does not allow any proper size, weight, or cost analysis at the vehicle level".

Table 3 Stack global results

Parameter	Value	Unit
Input data		
Cell temperature	90	°C
Cell pressure	1	atm
Cell area	30	cm^2
Current density	100	mA/cm^2
Cell fuel utilization factor	0.95	
Stack tension	48	V
Results		
Cell tension	0.333	V
Cell overpotential (total)	0.804	V
Cell power density	3.33	mW/cm^2
Cell efficiency	0.2678	
Number of cells in a module	145	
Module power density	4.8	W/cm^2
Module power	144	W
Number of modules in a stack	591	
Stack power	85	kW
Stack heat rejection (overpotential)	205.5	kW
Estimated stack area	1.8	m^2

Waste heat analysis is carried out through energy and exergy balances performed from results presented in Table 5. Sankey diagram presented in Fig. 8 graphically represents the energy balance of the stack. It shows that 28.8% of the enthalpy provided by the global reaction (Eq. 3) is converted to power; 68.2% corresponds to waste heat related to overpotential; and 5.4% corresponds to waste heat related to the gases and water exhausted from the stack. Unreacted ethanol is considered 5.0% from the total inlet ethanol, and it is not accounted in the energy and exergy balances, because it is recycled after cooling. Heat related to the cooling of the unreacted ethanol is only 0.2% of the energy provided by the global reaction.

Exergy balance graphically represented in Fig. 9 is the Grassman diagram of the stack, which shows that the power generated by the stack represents 28.1% of the fuel exergy. It also shows that 12.1% of the fuel exergy is available for power generation from overpotential waste heat, resulting in 36.8 kW of power generated through a Carnot cycle. In the same way, heat related to the reaction products corresponds to only 3.9% of the fuel exergy, so that a Carnot cycle using this stream as heat source would generate 11.8 kW of power. Nearly all the rest of fuel exergy (55.9%) is destroyed, i.e., converted irreversibly into heat. Thus, a rational efficiency of 46.2% is found.

Despite exergy analysis reveals a potential for power generation of 36.8 and 11.8 kW from overpotential and exhaust gases, respectively, it is not feasible, because the respective temperatures are very low for practical purposes. Furthermore, this potential for power generation is a theoretical higher limit, since it is grounded in Carnot machines. Actual thermal machines, on the other hand, are far more inefficient, especially for such small capacities. Thus, power generation from heat rejected by the stack quite likely does not pay off the inefficiency, weight, and bulk of an actual thermal machine.

Exergy analysis also shows that most of the heat generated in the stack is due to irreversibility, which is closely related to the heat generated by the cell overpotentials. Thus, a natural approach would be reducing the irreversibility by increasing the fuel cell voltage. However, a higher cell voltage also means lower current density and, consequently, a heavier and bulkier stack, which is not desirable in aircraft application.

A more practical alternative is the use of heat exchangers to recover part of the stack waste heat for cabin heating [12]. Low-temperature air from outside is heated and conveyed to the cabin. If stack waste heat is larger than the thermal demand for cabin heating, the exceeding heat is discarded to the atmosphere. This solution avoids the power demand related to cabin heating and, as a consequence, requires a smaller capacity stack, which is lighter and less bulky. A smaller stack also consumes less fuel, so

Table 4 Thermodynamic state of each stream of the stack

i	T [K]	$\dot{m}$ [kg/s]	$\dot{n}$ [kmol/s]	$\bar{h}$ [kJ/kmol]	$\bar{s}$ [kJ/kmolK]	$\bar{e}_{ph}$ [kJ/kmol]	$\bar{e}_{ch}$ [kJ/kmol]	$\bar{e}$ [kJ/kmol]
1	298	0.02325	0.0009300	7.025	0.03010	0	543.2	543.2
2	298	0.1523	0.005281	0	0.2324	0	1.874	1.874
3	363	0.03029	0.0007087	− 199.2	0.1115	0.1956	22.50	22.70
4	363	0.1443	0.005559	4.538	0.2321	0.3699	1.480	1.850
5	363	0.02913	0.0006620	− 201.9	0.1143	0.1247	10.41	10.53
6	363	0.1735	0.006223	− 50.00	0.2091	0.3197	3.906	4.226
7	363	0.0116	0.0004640	31.54	0.1015	3.215	543.2	546.4
8	298	0.0116	0.0004640	7.025	0.0301	0	543.2	543.2

Table 5 Composition of each stream of the stack

i	M	X_j				
	[kg/kmol]	EtOH	H_2O	CO_2	O_2	N_2
1	25.00	0.25	0.75			
2	28.84				0.21	0.79
3	42.74	0.0164	0.0492	0.934		
4	25.96		0.238		0.0893	0.672
5	44.00			1.0		
6	27.88		0.213	0.106	0.0798	0.601
7	25.00	0.25	0.75			
8	25.00	0.25	0.75			

that the aircraft would carry less ethanol if a DEPFC-based stack is used as APU.

In the conventional aircraft, it is common to cool down the oil from gearboxes using jet fuel as coolant. This is a synergetic solution, since it is necessary to avoid jet fuel freezing due to the very low air temperature in high altitude flights. However, more electric aircraft does not require as many gearboxes as the conventional ones. Thus, there is not much oil to cool down, but the need to avoid jet fuel freezing remains. When using a stack as APU in a more electric aircraft, part of stack waste heat can be used to heat the jet fuel through a heat exchanger.

Regarding the heat related to stack exhaust, the proposed alternative is to recover the hot water for use in lavatory or for human consumption [10], which requires cooling. In any case, this water should be treated to remove acetic acid and acetaldehyde resulting from actual stack operation. Since water from stack can be recovered, the aircraft can carry less fresh water for the flight. Figure 10 depicts the scheme to manage the stack waste heat based on the alternatives previously discussed.

Sankey and Grassman diagrams for the scheme depicted in Fig. 10 are presented in Figs. 11 and 12, respectively. In this scheme, stack is sized for 65 kW of power, since thermal demand for cabin heating (20 kW) is met through stack waste heat recovery. In this scheme, total waste heat is about 157 kW, so that 137 kW is available for jet fuel heating. Ethanol consumption corresponds to 241 kW. According to the Grassman diagram in Fig. 12, all the exergy from waste heat related to stack overpotentials can be recovered onboard the aircraft (cabin and fuel heating). This stack would require 452 modules. In a similar arrangement, it results a vertical array of 7 per 7 modules

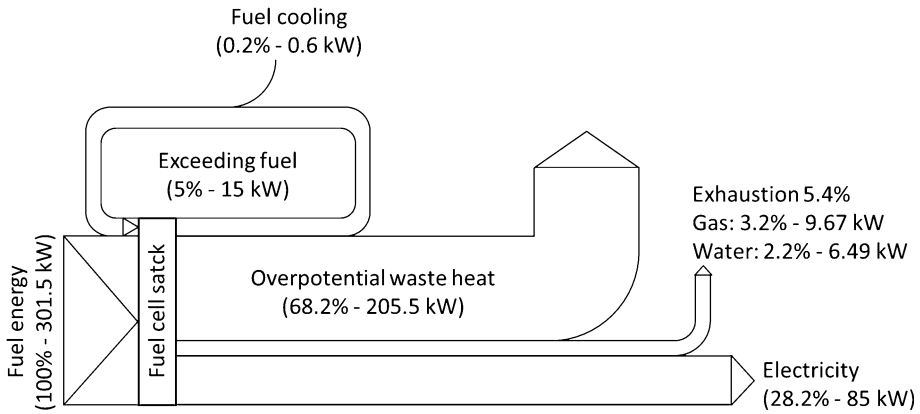

Fig. 8 Sankey diagram of the stack

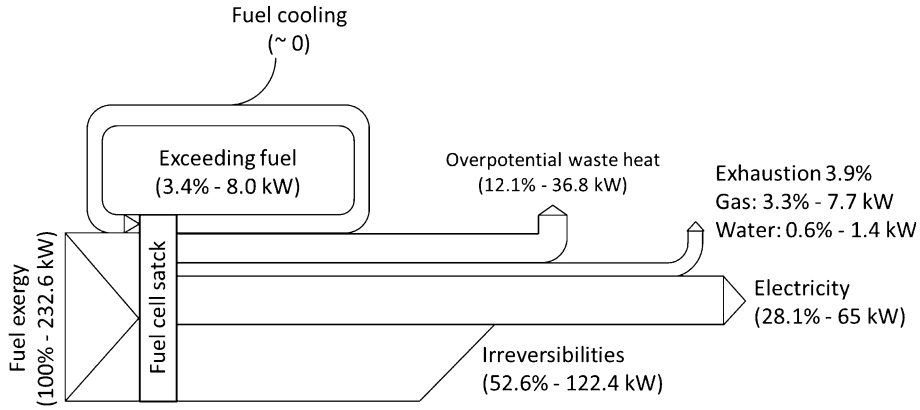

Fig. 9 Grassman diagram of the stack

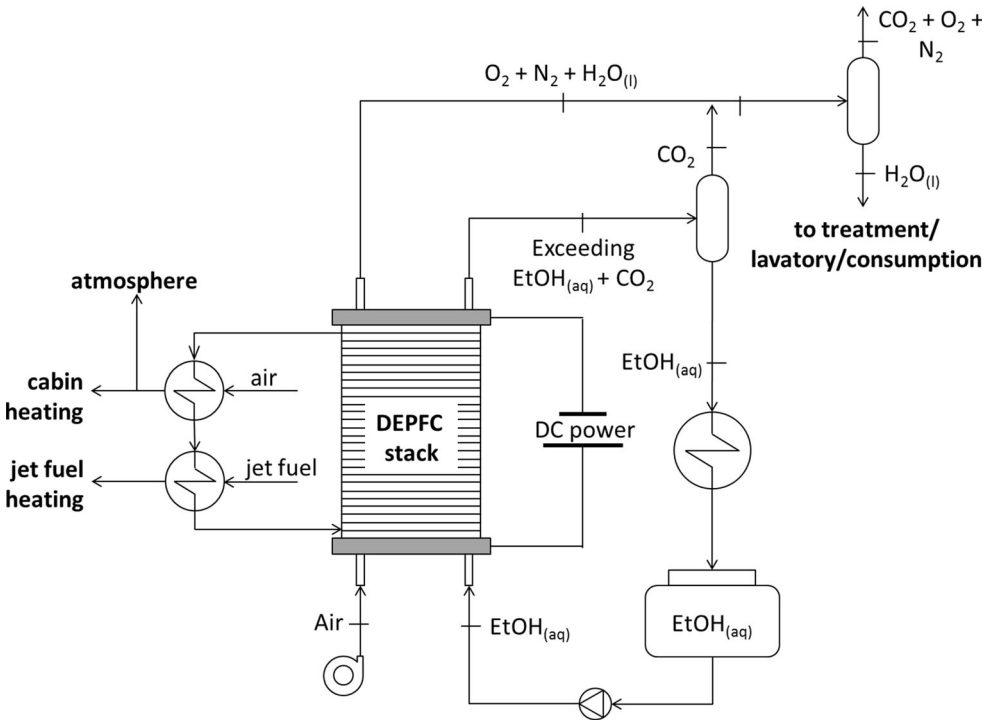

Fig. 10 Proposed scheme for stack waste heat management

piled horizontally in 10 columns. Each cell would have a total thickness of 0.8 mm, still not enough to accommodate the whole stack in a typical APU nacelle [18].

Figure 13 compares ethanol consumption between an 85 kW stack with no heat recovery (Fig. 4) and a 65 kW one with heat recovery (Fig. 10) for each stage of the flight (Fig. 2). The 65 kW stack with heat recovery consumes around 92 kg of ethanol in this flight, 31% less than the 85 kW stack without heat recovery (around 134 kg). In the same way, Fig. 14 compares water generation between the 85 kW stack and the 65 kW one: the first produces 314 kg of water during the whole flight and the last produces 217 kg. Maximum water demand onboard aircraft can be estimated in 51 kg/h [15]. The 85 kW stack exceeds these demand, so that water should be discarded. The 65 kW stack cannot assure this demand, but the gap is small. Interesting enough, it is worth noting that the aircraft would no longer need to carry large amounts of fresh water for onboard consumption.

Regarding jet fuel heating, its melting point is about − 47 °C, very close to the standard outside air temperature at 9000 m (− 44 °C). By recovering 205.5 kW of waste heat from the 85 kW stack, it is possible to heat 9.69 kg/s of jet fuel from − 47 °C to − 37 °C (Eq. 40, $c_{p,-jet} = 2.121$ kJ/kgK). In a similar way, the 65 kW stack provides 137.1 kW of waste heat, which could heat 6.20 kg/s of jet fuel to − 37 °C. At cruise speed, average fuel consumption of the Dornier 328 jet can is approximately 28 g/km/passenger or 0.150 kg/s, according to the International Council of Clean Transportation (ICCT). Thus, from a thermodynamic point of view, both stack configurations could avoid fuel freezing in cruise altitude.

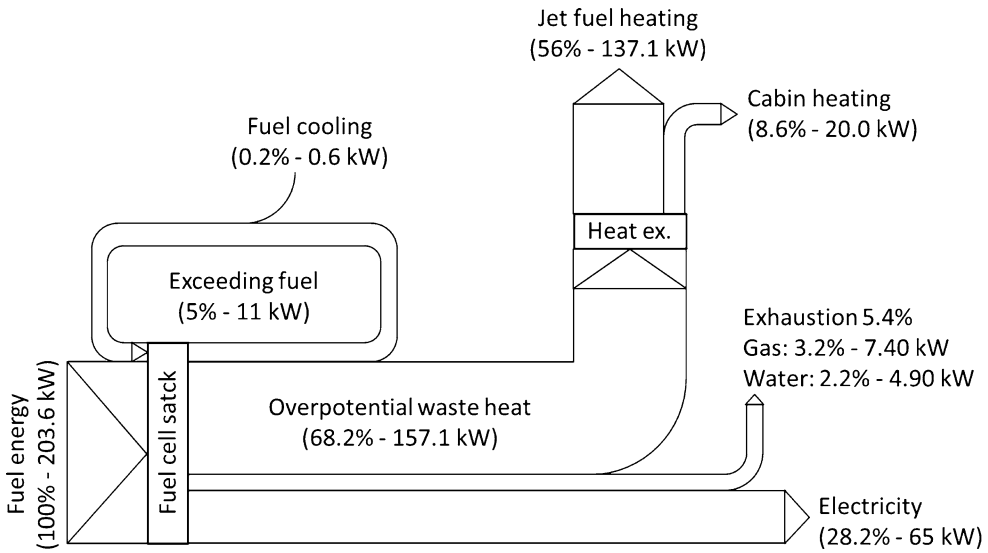

Fig. 11 Sankey diagram for the scheme presented in Fig. 10

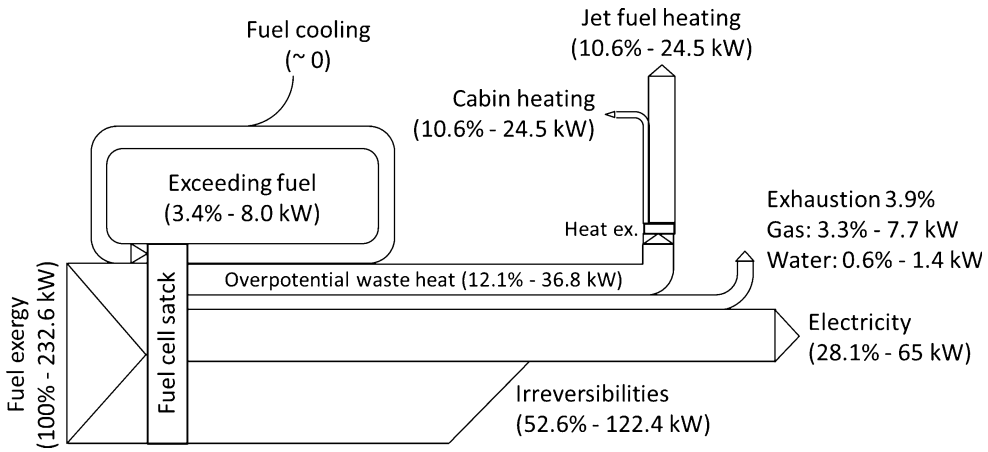

Fig. 12 Grassman diagram for the scheme presented in Fig. 10

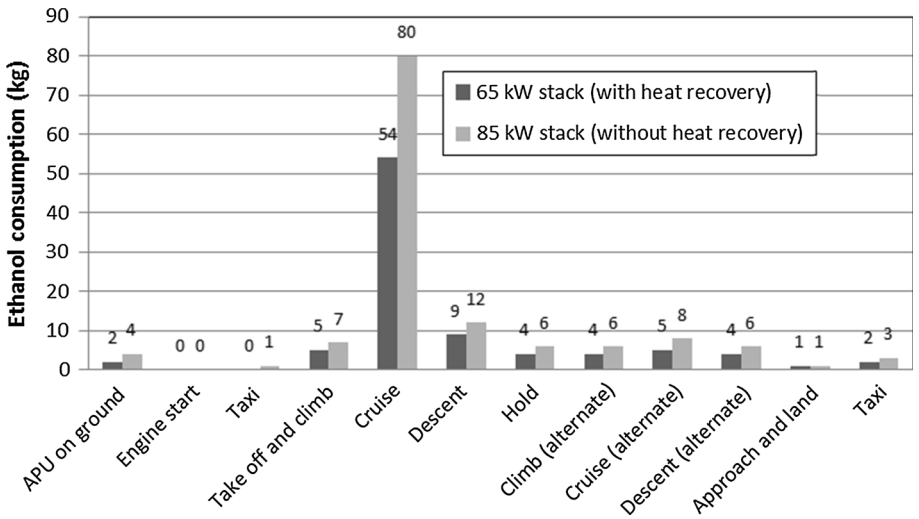

Fig. 13 Comparison of ethanol consumption

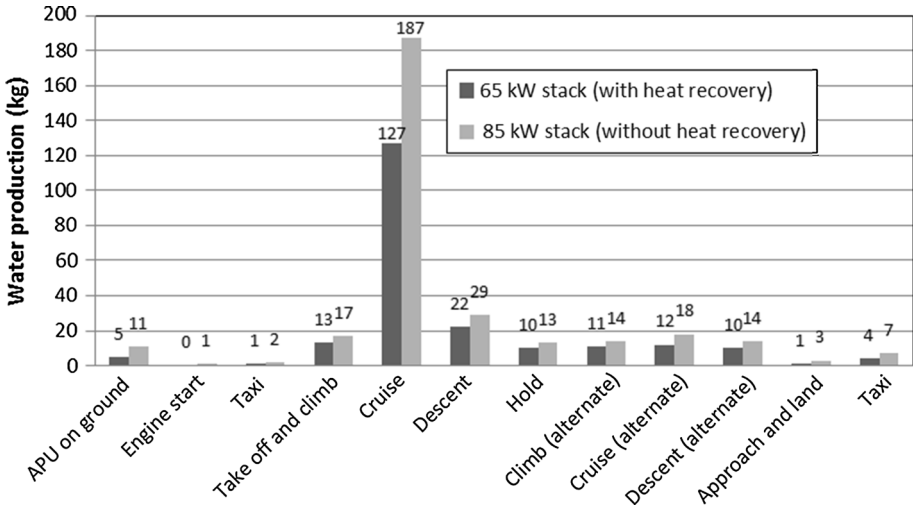

Fig. 14 Comparison of water production

A detailed analysis regarding the heat exchanger design for that is necessary, especially regarding its weight and volume, but it is out of the scope of the present work:

$$\dot{m}_{\text{jet}} = \frac{\dot{Q}_{\text{stack}} - \dot{Q}_{\text{cabin}}}{c_{\text{p,jet}} \Delta T}. \tag{38}$$

4 Conclusion

The use of a stack based on direct ethanol polymer fuel cell as APU of a more electric jet aircraft was proposed, since the literature presents for this application alternatives based on hydrogen fuel cells, particularly PEMFC (polymer electrolyte membrane fuel cell) and SOFC (solid oxide fuel cell). Cell was modelled to predict its performance and good results were found when compared to experimental data available in the literature. A current density equal to 100 mA/cm^2 was chosen, because cell operation around this value is a trade-off between higher current density that makes the stack less heavy and bulky, and lower current density that make the stack more efficient. At this point, the stack could not fit into a standard APU nacelle due to the cell thickness. Exergy analysis of the stack showed that at low current densities, i.e., higher cell voltages, the irreversibility are smaller. Exergy analysis also revealed that recovering the heat related to cell overpotential is feasible for cabin heating and jet fuel heating, but it is highly unpractical for power generation. Heat recovering allowed sizing a smaller stack, because no power is no longer required for cabin heating. Hot water produced by the stack could also be recovered for use in the lavatory or for human consumption, after proper treatment. Onboard production of water is interesting, since the aircraft would not need to carry fresh water for onboard consumption. Besides the technical aspects, DEPFC as APU may promote the use of renewable fuel in the aviation industry in a way that virtually no NOx emission is observed, which is not possible in the conventional APU based on thermal engines. Despite DEPFC technology is still not mature, it can be concluded that it is a promising and more sustainable alternative for use as APU in more electric aircraft. The research of more efficient cells is to be continued to increase cell voltage and efficiency, and to reduce the size and weight as well.

References

1. Lee DS, Pitari G, Grewe V, Gierens K, Penner JE, Petzold A, Prather MJ, Schumann U, Bais A, Berntsen T, Iachetti D, Lim LL, Sausen R (2010) Transport impacts on atmosphere and climate: aviation. Atmos Environ 44(37):4678–4734. https://doi.org/10.1016/j.atmosenv.2009.06.005
2. Psanis C, Triantafyllou E, Giamarelou M, Manousakas M, Eleftheriadis K, Biskos G (2017) Particulate matter pollution from aviation-related activity at a small airport of the Aegean Sea Insular Region. Sci Total Environ 596–597:187–193. https://doi.org/10.1016/j.scitotenv.2017.04.078
3. Wasiuk DK, Khan MAH, Shallcross DE, Lowenberg DH (2016) The impact on tropospheric composition changes of global aviation NOx emissions from 2005 to 2011. Atmos Res 2016. https://doi.org/10.1016/j.atmosres.2016.03.012
4. Kyprianidis KG, Dahlquist E (2016) On the trade-off between aviation NOx and energy efficiency. Appl Energy. https://doi.org/10.1016/j.apenergy.2015.12.055
5. Kim T, Kwon S (2012) Design and development of a fuel cell-powered small unmanned aircraft. Int J Hydrog Energy 37(1):615–622. https://doi.org/10.1016/j.ijhydene.2011.09.051
6. Romeo G, Borello F, Correa G, Cestino E (2013) ENFICA-FC: design of transport aircraft powered by fuel cell & flight test of zero emission 2-seater aircraft powered by fuel cells fueled by hydrogen. Int J Hydrog Energy 38(1):469–479. https://doi.org/10.1016/j.ijhydene.2012.09.064
7. Fernandes A, Woudstra T, Aravind PV (2015) System simulation and exergy analysis on the use of biomass-derived liquid-hydrogen for SOFC/GT powered aircraft. Int J Hydrog Energy

40(13):4683–4697. https://doi.org/10.1016/j.ijhydene.2015.01.136
8. Kim T (2014) NaBH4 (sodium borohydride) hydrogen generator with a volume-exchange fuel tank for small unmanned aerial vehicles powered by a PEM (proton exchange membrane) fuel cell. Energy 69:721–727. https://doi.org/10.1016/j.energy.2014.03.066
9. Terörde M, Lücken A, Schulz D (2013) Weight saving in the electrical distribution systems of aircraft using innovative concepts. Int J Energy Res 38(8):1075–1082. https://doi.org/10.1002/er.3116
10. Keim M, Kallo J, Friedrich KA, Werner C, Saballus M, Gores F (2013) Multifunctional fuel cell system in an aircraft environment: an investigation focusing on fuel tank inerting and water generation. Aerosp Sci Technol. https://doi.org/10.1016/j.ast.2013.04.004
11. Pratt JW, Klebanoff LE, Munoz-Ramos K, Akhil AA, Curgus DB, Schenkman BL (2013) Proton exchange membrane fuel cells for electrical power generation on-board commercial airplanes. Appl Energy 101:776–796. https://doi.org/10.1016/j.apenergy.2012.08.003
12. Santarelli M, Cabrera M (2011) Hybrid solid oxide fuel cell and micro gas turbine for regional jets. J of Airc 48(4):1216–1224. https://doi.org/10.2514/1.C031228
13. Samsun RC, Pasel J, Peters R, Stolten D (2015) Fuel cell systems with reforming of petroleum-based and synthetic-based diesel and kerosene fuels for APU applications. Int J Hydrog Energy 40(19):6405–6421. https://doi.org/10.1016/j.ijhydene.2015.03.091
14. Zakil FA, Kamarudin SK, Basri S (2016) Modified Nafion membranes for direct alcohol fuel cells: an overview. Renew Sustain Energy Rev 65:841–852. https://doi.org/10.1016/j.rser.2016.07.040
15. An L, Zhao TS, Li YS (2015) Carbon-neutral sustainable energy technology: direct ethanol fuel cells. Renew Sustain Energy Rev 50:1462–1468. https://doi.org/10.1016/j.rser.2015.05.074
16. Pramanik H, Basu S (2010) Modeling and experimental validation of overpotentials of a direct ethanol fuel cell. Chem Eng Process 49(7):635–642. https://doi.org/10.1016/j.cep.2009.10.015
17. Andreadis GM, Podias AKM, Tsiakaras PE (2008) The effect of the parasitic current on the Direct Ethanol PEM Fuel Cell Operation. J Power Sources 181(2):214–227. https://doi.org/10.1016/j.jpowsour.2008.01.060
18. Abdullah S, Kamarudin SK, Hasran UA, Masdar MS, Daud WRW (2015) Development of a conceptual design model of a direct ethanol fuel cell (DEFC). Int J Hydrog Energy 40:11943–11948. https://doi.org/10.1016/j.ijhydene.2015.06.070
19. Goel J, Basu S (2015) Mathematical modeling and experimental validation of direct ethanol fuel cell. Int J Hydrog Energy 40:14405–14415. https://doi.org/10.1016/j.ijhydene.2015.03.082
20. Sousa RJ, Anjos DM, Tremiliosi-Filho G, Gonzalez ER, Coutanceau C, Sibert E, Léger JM, Kokoh KB (2008) Modeling and simulation of the anode in direct ethanol fuel cells. J Power Sources 180:283–293. https://doi.org/10.1016/j.jpowsour.2008.01.048
21. Kamarudin MZF, Kamarudin SK, Masdar MS, Daud WRW (2012) Review: direct ethanol fuel cells. Int J Hydrog Energy 38(22):9438–9453. https://doi.org/10.1016/j.ijhydene.2012.07.059
22. Kotas TJ (2012) The exergy method of thermal plant analysis. Paragon Publishing, Trowbridge
23. Suresh NS, Jayanti S (2011) Cross-over and performance modeling of liquid-feed polymer electrolyte membrane direct ethanol fuel cells. Int J Hydrog Energy 36(22):14648–14658. https://doi.org/10.1016/j.ijhydene.2011.07.105
24. Berg H, Nyman J, Erlandsson P, Johansson P, Matic A (2015) Direct Ethanol Fuel Cells: Ethanol for our future fuel cells? Energiforsk technical report 137. https://energiforskmedia.blob.core.windows.net/media/18529/direct-ethanol-fuel-cells-ethanol-for-our-future-fuel-cells-energiforskrapport-2015-137.pdf. Accessed 11 Nov 2017